All-optical control of quantized momenta on a polariton staircase

M. Aßmann, F. Veit, and M. Bayer
Experimentelle Physik 2, Technische Universität Dortmund, 44221 Dortmund, Germany

A. Löffler, S. Höfling, M. Kamp, and A. Forchel
Technische Physik, Physikalisches Institut, Wilhelm Conrad Röntgen Research Center for Complex Material Systems, Universität Würzburg, D-97074 Würzburg, Germany

(Received 3 January 2012; revised manuscript received 13 April 2012; published 24 April 2012)

Here we demonstrate a simple and reconfigurable way to create a polariton condensate in well defined discrete momentum states, allowing us to manipulate the local polariton flow. To this end, we created a spatially varying potential formed in the presence of noncondensed carriers by subjecting a microcavity to spatially modulated nonresonant optical excitation. The choice of the spatial shape of this potential allows us to tailor the properties of the polariton condensate in momentum space. Our results demonstrate a way to prepare a polariton condensate in an adjustable momentum state and provide a first step toward the creation of functional all-optical elements for polaritonic logic circuits on demand by projecting circuits onto an unprocessed planar sample.

DOI: 10.1103/PhysRevB.85.155320 PACS number(s): 71.36.+c, 42.65.Sf, 78.47.D−, 78.55.Cr

I. INTRODUCTION

All-optical logic circuits are promising alternatives to electronic circuits,[1] and their advantages and drawbacks are heavily discussed.[2,3] Recently much research has been devoted especially to exciton-polariton based designs due to their efficient coupling to external light fields and possible applications of polariton condensates in terms of opto-spintronics.[4–6] The problems that need to be considered in realizing polariton-based circuits are efficient designs for gates and switches,[7,8] transistors[9,10] and other functional elements, linking of several logic elements,[11,12] and preparation of the system in well defined states.

Polaritons are composite bosons, and it has been shown that a system of a macroscopic number of polaritons in a single state shows several signatures of Bose-Einstein condensates (BECs)[13] and related features such as superfluidity[14] and persistent currents,[15] which can be maintained at elevated temperatures. Due to their short lifetime, polaritons form a kind of dynamical BEC. It has been suggested to exploit these special characteristics to build polaritonic logic circuits. Such circuits need two main prerequisites: long coherence lengths to create extended condensates and the possibility to create arbitrary potentials to form functional elements and devices.[16] While long coherence lengths have already been demonstrated elsewhere,[17] potentials have so far mostly been realized using lithographic means such as using patterned microcavities[18] or depositing thin metal films on top of them.[19,20] These techniques are able to create well defined potentials, but they are necessarily static and determined at the time of processing the sample. Further techniques include strain[21] and acoustic lattices[22] which, however, do not allow for reconfigurable circuits. Recently, all-optical techniques, introducing potentials by exploiting either the repulsive interaction of polaritons of different spin[23,24] to create barriers for flowing polaritons or the repulsive interaction with carriers created by nonresonant optical pumping,[17,25] have been realized for simple, typically Gaussian geometries. Using all-optical techniques, one of the great advantages of polaritonic circuitry lies in the opportunity to create arbitrary potentials and therefore also optically projected circuits, which can be tailored by changing the shape of the excitation on demand optically.

II. EXPERIMENTAL SETUP

In this work, we use nontrivial potential landscapes to directly tailor the externally accessible momentum space properties of a polariton condensate. We demonstrate the capabilities of this approach by realizing a polariton BEC populating several discrete linear momentum states in a given direction. Under nonresonant excitation the presence of noncondensed particles produces a mean-field repulsive potential, much larger than those created when using resonant excitation schemes, that matches the shape of the excitation spot.[26] If this potential varies in space, two scenarios are possible. Either desynchronized condensates at different energies form[27] or one single condensate forms and the energy difference at different spatial positions vanishes either due to polariton Josephson currents[28] or due to modulation of the local condensate wave vector $\vec{k}_c(\vec{r})$.[26] We use the latter effect to tailor the momentum-space distribution of a polariton condensate. A sensible mean-field description of the condensate dynamics can be obtained from a generalized Gross-Pitaevskii equation in the local density approximation.[26] For simple Gaussian geometries one finds the result that repulsive interactions create an antitrapping potential that causes ballistic acceleration of the condensate polaritons towards the edge of the condensate. Under steady-state conditions the condensate state is given by the following state equation:

$$\hbar(\omega_c - \omega_{LP}) = \frac{\hbar^2 k_c^2(\vec{r})}{2m} + \Delta E(\vec{r}). \tag{1}$$

Here $\hbar\omega_c$ and $\hbar\omega_{LP}$ give the energies of the condensate and the minimum of the lower polariton band, respectively, m represents the lower polariton mass, and k_c is the local condensate wave vector. ΔE denotes the spatially varying blueshift the condensed polaritons experience due to interactions. This blueshift arises due to polariton-polariton interactions, local modulations of the the ground state energy due to disorder, and interactions with the reservoir of carriers created by

pumping like electrons, holes, or excitons. The latter is usually the dominant contribution to the blueshift for nonresonant excitation. The magnitude of the blueshift is proportional to the locally varying pump intensity under continuous pumping. If the condensate forms a single state, the condensate responds to the local variation in $\Delta E(\vec{r})$ by acquiring a local change in k_c such that Eq. (1) is fulfilled. Given the boundary condition that k_c vanishes at the position of maximum pump intensity, Eq. (1) already determines the condensate energy and wave-vector modulus for a given pump geometry:

$$|k_c(\vec{r})| = \sqrt{\frac{2m[\hbar(\omega_c - \omega_{LP}) - \Delta E(\vec{r})]}{\hbar^2}}. \quad (2)$$

In our experiments the sample is held at 8 K and consists comprehensively of 12 GaAs/AlAs quantum wells embedded in a planar microcavity with 16 (20) AlGaAs/AlAs mirror pairs in the top (bottom) distributed Bragg reflector. To study the spatially, spectrally, and time resolved emission a liquid crystal tunable filter with spectral resolution of 0.75 nm, a liquid-nitrogen-cooled CCD and a synchroscan streak camera with temporal resolution of ≈2–3 ps were used. For calculations the polariton mass was assumed to be $5\times10^{-5}m_e$, where m_e gives the free-electron mass. We used nonresonant pulsed excitation using a Ti:Sa laser with a pulse duration of 2 ps and a spatial light modulator (Holoeye-Pluto) to create a quasi-one-dimensional wire staircase potential consisting of 16 steps of 1 μm length each. The experiments were carried out at zero detuning. More detailed information on the sample and a detailed characterization of the emission properties in the uncondensed, condensed, and lasing regimes can be found in Refs. 29 and 30. Each step of the imprinted potential defines a plateau of constant pump intensity and the intensity at the nth plateau is given by a fraction $(1 - \frac{n}{16})I_0$ of the maximum intensity I_0, where $n = 0, \ldots, 15$ in our case. At the position of the highest intensity also the highest blueshift E_0 is found. In the direction orthogonal to the potential staircase, the width of the pumping spot is ≈2 μm. While there is no trapping potential that keeps the condensate from extending beyond this region, the limited pump spot and polariton lifetime cause it to become gain-trapped.[31] For this geometry Eq. (2) becomes

$$|k_c(\vec{r}_n)| = \sqrt{\frac{2m\left[E_0 - \left(1 - \frac{n}{16}\right)E_0\right]}{\hbar^2}} = \sqrt{\frac{2mE_0}{16\hbar^2}}\sqrt{n}, \quad (3)$$

so that the modulus of the wave vector is expected to be the same at each position on a plateau. The shape we imprinted on the excitation spot is shown in Fig. 1. The corresponding energy-integrated real-space emission pattern and the intensity profile along the staircase gradient direction can be seen in Fig. 1. Due to diffraction, the emission pattern shows some deviations from the ideal shape. The consequences and perspectives for improvement will be discussed later. There is still a significant amount of emission at distances up to 20 μm away from the pump spot, which indicates expansion of the polaritons.

Within the range of experimental parameters applied here a single condensate state forms (see Sec. III). Its shape in momentum space is determined by the local shape of the pump spot as suggested by Eq. (3). The momentum-space

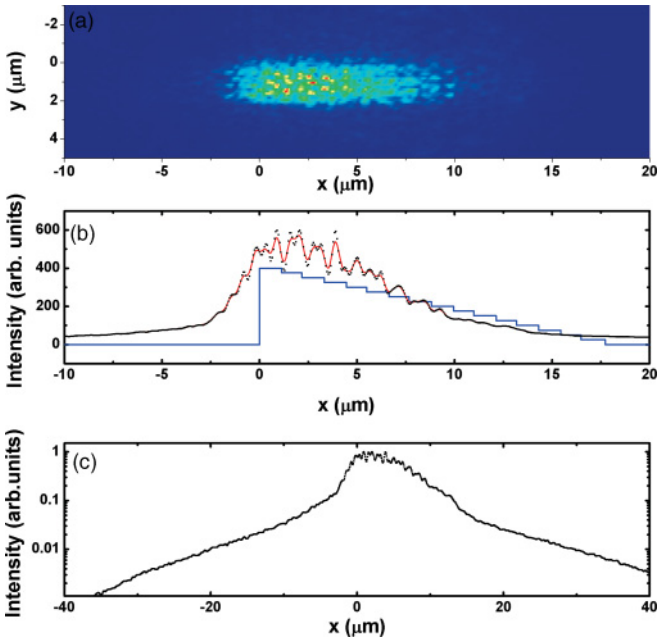

FIG. 1. (Color online) (a) Real-space shape of the excitation spot used. (b) Intensity profile integrated along the y axis. The red line gives a three-point-smoothed guide to the eye. The blue line gives the target spatial shape of the excitation spot used as the input for the SLM. (c) Normalized real-space intensity profile integrated along the y axis on a logarithmic scale. There is still a significant amount of emission up to 20 μm away from the steep edge of the staircase potential, indicating polariton expansion away from the pump spot.

distribution of the condensate density at a detection energy centered around 7.3 meV above the lower polariton energy of 1.6060 eV is shown in the upper right panel of Fig. 2 for an excitation density of roughly four times the threshold density P_{thr}. The polariton density is peaked along several discrete values in the direction of k_x, which corresponds to wave vectors oriented along the polariton staircase potential. These maxima form spontaneously as the condensate forms as can be seen in the momentum-space distribution of the lower polariton shown in the upper left panel of Fig. 2.

Here, the distribution is broad and no peaks are visible at all. In order to demonstrate that it is indeed the presence of the antitrapping background potential that causes momentum quantization of the polariton condensate in the x direction, we extracted the positions of the polariton density maxima in momentum space and plotted them against the index number of the corresponding maximum. The result is shown in the lower right panel of Fig. 2. The dependence matches nicely the square-root dependence that is expected for a staircase potential with linear step size. The solid line gives a power-law fit to the function

$$k_x(n) = a(n - n_0)^p. \quad (4)$$

The resulting fit parameters are shown in the figure. Parameter a directly allows us to estimate the blueshift of the condensate compared to the LP to 7.4 meV with higher precision than just by using our tunable spectral filter, which has a spectral width of 0.75 nm (≈1.2 meV). It should be noted that an

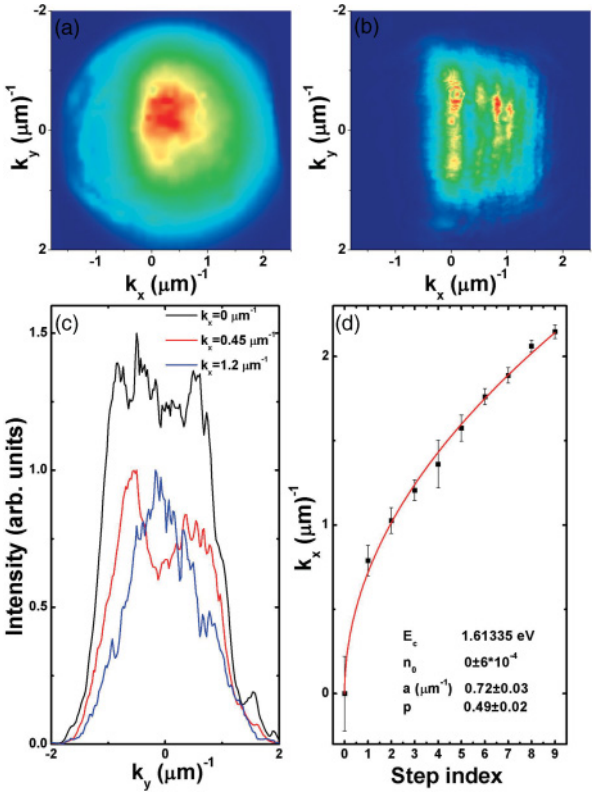

FIG. 2. (Color online) (a) Polariton momentum-space pattern of the uncondensed lower polariton branch. (b) Polariton momentum-space pattern in the condensed regime. Discrete momentum states occur in the k_x direction. (c) Intensity distribution along k_y for three values of k_x in the condensed regime. The line at $k_x = 0.45\ \mu\text{m}^{-1}$ shows a double-peaked shape and differs significantly from the other lines. (d) Center positions of the maxima in momentum space seen in the condensed regime. The solid line gives a power-law fit unambiguously showing the square-root dependence.

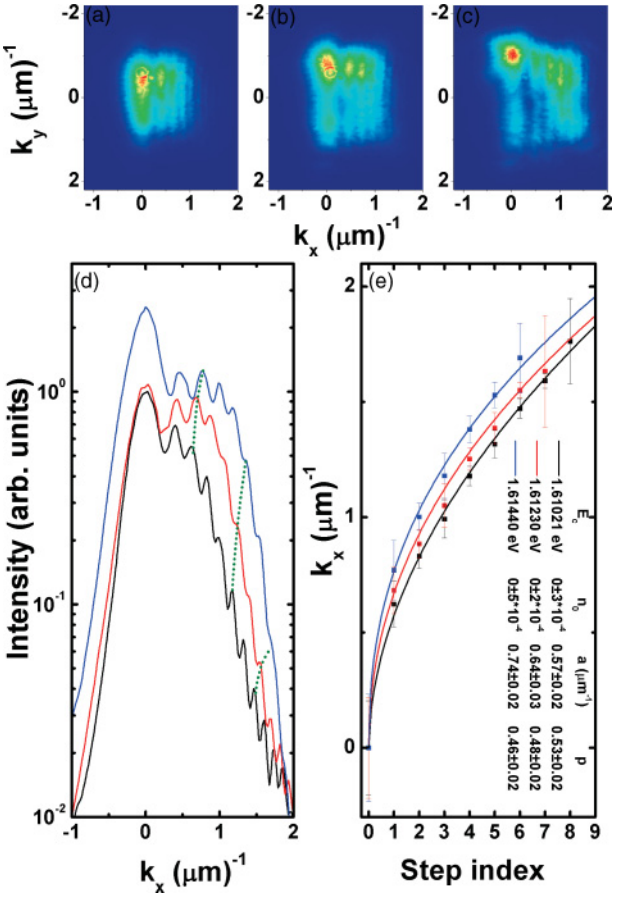

FIG. 3. (Color online) (a)–(c) Polariton momentum-space distributions in the condensed regime at central energies of 4.2, 6.3, and 8.4 meV above the lower polariton ground state. (d) Polariton momentum-space distributions corresponding to (a) (black), (b) (red) and (c) (blue) integrated along k_y. Green-dashed lines indicate the maxima with index numbers 1, 4, and 6, respectively. (e), Center positions of the maxima in momentum space. The solid lines represent power-law fits.

additional emission maximum is visible at $k_x \approx 0.45\ \mu$m. Its momentum-space intensity distribution differs strongly from the other lines, as shown in the lower left panel of Fig. 2, and it can most probably be traced back to momentum redistribution of polaritons belonging to the first line (see Sec. V).

To demonstrate the tunability of our design we also measured the time-integrated momentum-space polariton distribution at a different sample position and higher excitation density of ten times P_{thr} for different emission energies. Results are shown in the upper panel of Fig. 3 for (from left to right) energy windows centered around 1.61021, 1.61230, and 1.61440 eV. The stripe pattern in momentum space is comparable to the one seen for lower excitation density at the lowest energy. At higher energies two differences are evident: The stripe distance increases for higher energies and the polariton density is redistributed from $k_y = 0$ toward larger values of k_y. The first effect can be seen in more detail in the lower panels of Fig. 3, which show cuts through the intensity distributions along $k_y = 0$ and the positions of the maxima in momentum space versus their index number, respectively. While the maxima at $k_x = 0$ coincide for all three energies, the maxima with higher index number tend to shift to higher momentum values for larger step sizes as shown by dashed green lines for the maxima with index numbers 1, 4, and 6, respectively. The solid lines in the lower right panel are power-law fits to the positions of the maxima which give the fit parameters indicated in the plot. All three curves show only small deviations from ideal square-root behavior. The shift of the positions of the maxima can be explained when taking into account that the background carrier population will be highest after the excitation pulse and decrease afterwards. Accordingly the emission energy shifts toward smaller values as the background carrier number decreases. The momenta the condensed polaritons acquire at each of the steps of the staircase potential also decreases, which demonstrates nicely that the momentum-space distribution is indeed tunable by varying the imprinted potential. The fit values correspond to blueshifts of 4.7, 5.9, and 7.9 meV from the LP energy of 1.6060 eV, respectively. The emission energies are therefore identified as 1.6107, 1.6119, and 1.6139 eV, which is in good agreement with the central energies investigated.

Further interesting questions are why the momentum quantization occurs on discrete lines in momentum space and not on discrete momenta and why the polariton expansion

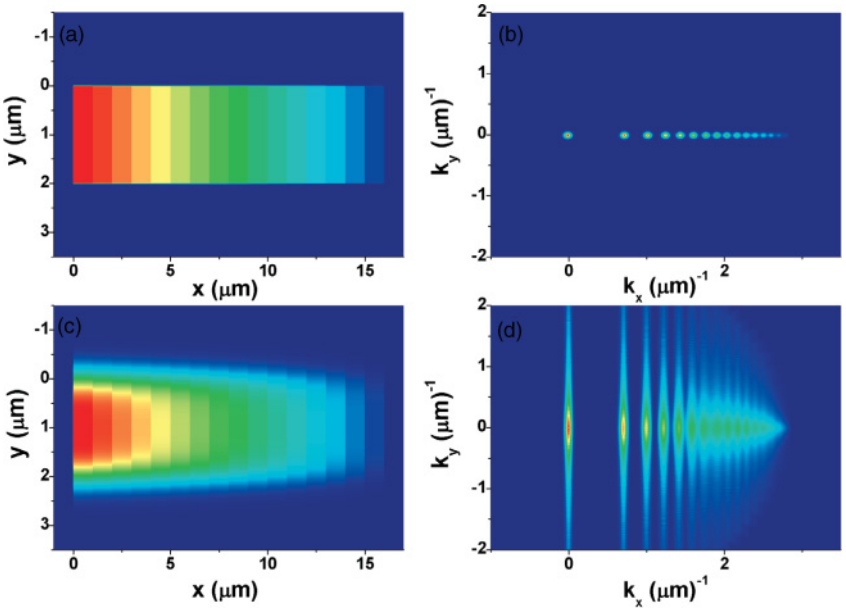

FIG. 4. (Color online) Real (a) and momentum-space (b) emission pattern of a polariton condensate created by an ideal staircase-shaped pumping spot taking only geometrical broadening into account. Real- (c) and momentum-space (d) emission pattern of a polariton condensate created by an imperfect staircase-shaped pumping spot taking only geometrical broadening into account. The smoothed edge along the y axis causes a large broadening in momentum space.

is anisotropic with more polariton flow into the k_y direction from the topmost step of the staircase as compared to the $-k_x$ direction. To explain this behavior it is necessary to take the small size of each potential step into account, which is only 2 μm^2. The small spot size in the direction perpendicular to the staircase potential may introduce two effects that can lead to significant broadening of the polariton distribution in momentum space: the fundamental broadening caused by position-momentum uncertainty and a broadening caused by imperfections of the shape of the potential due to diffraction. We will call the latter geometrical broadening in the following. In order to distinguish which component is dominant here, we calculated polariton distributions from a phenomenological model that only takes geometrical broadening into account. The results are shown in Fig. 4 (see Sec. IV). Here the upper panels show an ideal staircase potential and the momentum space distribution associated with it, while the lower panel gives the real-space and momentum-space distributions for a potential with blurred edges. The results shown in the lower panel are in good qualitative accordance with the experimental results in Fig. 2. Now we check whether the broadening is geometry or uncertainty limited. The 2 μm full-width-at-half-maximum step width corresponds to a standard deviation of the underlying real-space polariton distribution in the y direction of roughly $\sigma_x \approx 0.85$ μm for rectangular, sigmoidal, or Gaussian spot shapes. This allows us to determine the lower bound of the polariton wave-vector uncertainty in the y direction as $\sigma_k \geqslant 0.59$ μm^{-1}. For the simulated data in the lower panel of Fig. 4 and the experimental data the standard deviation of the polariton wave vector is at least 0.7 μm^{-1} or even larger, which shows that the broadening is larger than the limit imposed by uncertainty, and therefore geometrical broadening plays a role. For high pump densities, the effective spot slope in y direction tends to look like a Gaussian instead of a step, and polaritons are accelerated ballistically to the region outside the pump spot potential. This causes the intensity redistribution in the k_y direction observed in Fig. 3.[26] But it is also clear that the momentum broadening seen is close to the uncertainty limit and therefore the quality of the imprinted potential is sufficient. Nevertheless it should be noted that the estimate of the lower bound is a pessimistic one for the limit of very short polariton lifetimes. As the polaritons may move away from the pump beam the real spatial polariton distribution will be broader than the bare step width.

It is also interesting to estimate the step width one should aim for to reach the uncertainty limit for a perfectly imprinted potential, as shown in the upper panels of Fig. 4. In that case the typical geometrical broadening can be almost as small as 0.1 μm^{-1}, which already requires a spatial extent of roughly 10 μm (full width at half maximum) to reduce the uncertainty-limited broadening to a magnitude comparable to the geometrical broadening.

III. SYNCHRONIZATION

To check whether a polariton condensate at a single energy forms when a staircase-shaped spot is used or condensation occurs in several energy states at once, we performed a spatially, spectrally, and time-resolved analysis of the condensate emission. As can be seen in Fig. 5, at high excitation powers and earlier times when the blueshift is quite large several condensate modes can be present simultaneously (upper right panel). After an initial relaxation phase one common ground state develops for lower excitation densities (upper left panel). The energy of this state slowly decreases with time as the background carrier density decreases too (lower panels). For very high excitation densities the condensate may stay fragmented even at late times (lower right panel). This behavior arises most probably due to the system transiting into the weak coupling regime accompanied by the onset of lasing. While the background carriers need to relax spontaneously towards the polariton branches in the strong coupling regime, they can directly couple efficiently to the light field in the lasing regime. In the first case the background carrier population will decay with a constant rate everywhere, while in the latter case stimulated emission may cause spatial hole

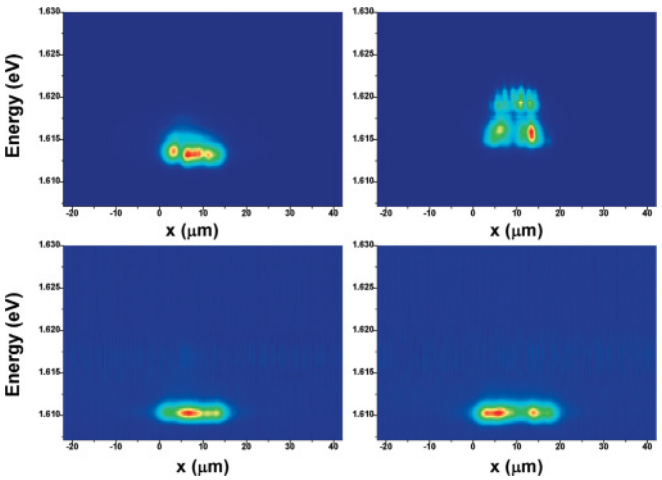

FIG. 5. (Color online) Spatially resolved real-space emission pattern emitted from the microcavity for pump densities below (left panel) and above (right panel) the transition to the weak coupling regime. The upper row shows the emission pattern at large blueshifts early in the pulse. The lower row gives the emission patterns at smaller blueshifts 90 ps (left side) or 120 ps (right side) later.

burning in the background carrier population, which actually strongly reshapes the potential. The formation of binding and antibinding states might also occur and change the emission. However, reliable identification of those might require cw pumping.

It should be further noted that the occurring blueshifts can be quite large, and it is interesting to consider the effects of the system transiting into the weak coupling regime. The system is expected to transit into the weak coupling regime approximately when the blueshift due to interactions becomes comparable to the energy difference between the lower polariton and the bare cavity mode. A more detailed study of the transition into the weak coupling regime under comparable experimental conditions on the same sample can be found in Ref. 29, where it has been shown that the transition occurs at a blueshift of roughly 7.7 meV under the conditions present in this experiment. While the results shown in Fig. 2 are taken at smaller blueshifts, the results shown in Fig. 3 are already more complicated. Here, the largest blueshift is roughly 8 meV. However, it is apparent that there is no emission from states with small k, but the emission comes from states with $k \neq 0$. Around $k = 0$ the major part of the blueshift arises due to Coulomb interactions, while for increasing k the kinetic energy also needs to be taken into account. At this point it is important to consider that only the blueshift due to Coulomb interactions is responsible for screening effects that reduce the exciton oscillator strength and in turn lead to breaking of the strong coupling regime, but not the kinetic energy. Therefore, the existence of a region without condensate emission in momentum space as seen most prominently in Fig. 3(c) is indeed expected, as the strong coupling regime would be broken near $k = 0$. Instead, the emission comes mainly from regions in momentum space where $|k|$ is at least 1 $\mu\mathrm{m}^{-1}$. In this region, the kinetic energy gained by the polaritons already amounts to roughly 1 meV, which in turn means that Coulomb interactions cause a blueshift around 7 meV, which is still below the transition to the weak coupling regime.

IV. THEORETICAL MODEL

We implemented a simple and phenomenological model to calculate the results for the geometrical broadening shown in Fig. 4. Starting from the state equation (1), it was first assumed that the contributions to the blueshift that are caused by the pump beam are dominant, and polariton-polariton interactions and disorder can be neglected or incorporated by slightly changing the shape of the assumed pump beam. Next, it was assumed that a local density approximation can be applied, which basically means that the system can be considered similar to a homogeneous system with a locally varying pump rate. Under such conditions the locally acquired wave vector depends solely on the local pump rate, and quantum pressure terms can be neglected. This approximation is not necessarily justified for a staircase potential, but effects beyond these approximations can be treated in terms of a modified pump spot. For calculating the momentum space distribution, we now assumed that the x and y components of the wave vector can be separated. The pump spot is divided into stripes along the y direction at fixed x positions. The value of k_x is assumed to be the same for each position inside the stripe and is determined by the difference between the highest pump density of the whole pump spot and the highest pump density inside the stripe. The value of k_y is then determined by the difference between the pump density at a given position and the highest pump intensity within its stripe. In the calculations for the momentum-space emission patterns shown in Fig. 4, sigmoidals have been used to model the plateaus. To simulate the imperfections in imaging the staircase, the edge steepness of these sigmoidals has been varied.

However, the maxima in momentum space are broader in the experiment compared to the calculations, which is caused by two main effects. First, the calculations neglect disorder in the sample, which is supposed to add some random value to the local wave vectors. Second, the spectral width of the tunable liquid crystal filter is above 1 meV. For pulsed excitation the condensate energy will slowly decrease with time and so will the distance between the lines in momentum space. Accordingly, the measured momentum-space distribution will give an average over all those distributions that correspond to condensate energies within the transmission window of the filter used, which also broadens the spectra. Also, diffusion of the background carriers which will also smooth the edges might have some effect. These effects could be reproduced by varying the edge steepness of the sigmoidals in the direction of the staircase independently of the edge steepness in the perpendicular direction. However, there is no fundamental physical insight that could be gained by doing so.

V. OPTIMIZATION

It is worthwhile to discuss how the performance of imprinting the spatially varying potential can be improved. The width of the maxima in momentum space could be reduced drastically by using continuous-wave instead of pulsed excitation, which would in turn require a microcavity

with a higher quality factor and lower threshold excitation density. The broadening could be further reduced for enlarged steps of equal intensity, as both the influence of diffraction on the edges and the influence of position-momentum uncertainty would be reduced. Also, using a two-dimensional staircase or pyramid potential would significantly improve the results. However, both approaches need higher coherence lengths and minimal disorder over a large area of the sample. While long coherence lengths have already been demonstrated,[17] disorder poses a serious problem because, even in samples with reduced disorder, cooling the sample to cryogenic temperatures already changes the disorder profile in an unpredictable manner. However, recently developed strategies to cancel the disorder potential[32] might solve this problem.

Along these lines it is also worthwhile to discuss the origin of the additional maximum visible in momentum space between the maxima with index numbers 0 and 1. However, this maximum differs significantly from the others as can be seen from the intensity distribution in k_y direction shown in the middle panel of Fig. 2. While the central maximum ($k_x = 0\ \mu\mathrm{m}^{-1}$) and those following the square-root dependence (e.g., $k_x = 1.2\ \mu\mathrm{m}^{-1}$) are symmetric around $k_y = 0\ \mu\mathrm{m}^{-1}$, the additional line shows a structure consisting of two peaks at finite values of k_y. These two peaks correspond to a total condensate wave vector of $|k_c(\vec{r})| \approx 0.7\ \mu\mathrm{m}^{-1}$, which is exactly the wave vector evidenced at the discrete line of index number 1. Therefore, this additional line most probably may be attributed to the maximum with index number 1, but has a momentum not completely aligned along the x axis. The additional line might also arise due to diffraction effects at the steep edge of the highest step of the polariton staircase. Diffraction-induced imperfections of the spot shape may create some additional small plateau. If such a plateau occurs, it will introduce emission on another line in momentum space. It is also possible that this maximum is created by elastic scattering of polaritons from the first plateau on a symmetric circle around $k = 0$. Further studies using cw excitation will be needed to clear this point up.

VI. CONCLUSION AND OUTLOOK

In conclusion, we show the potential of an all-optical scheme allowing one to tailor the momentum-space distribution of a polariton condensate by spatially varying nonresonant excitation. Discrete steps occur in momentum space, whose position can be tuned by adjusting the local excitation density. Our results provide a first step toward studies of momentum-sensitive all-optical switches and gates under well defined conditions. In this respect it is especially interesting that we are able to create directed asymmetric polariton flow. While it is easy to create directed polariton flow using resonant excitation, we have shown that control of the flow direction is also possible by means of nonresonant excitation. This directionality could, for example, be utilized for spatially selective switching by placing a staircase potential in between two regions pumped below the condensation threshold. Finally, we would like to point out that the potentials we used are also of major interest in experiments on polariton condensate flow in wire structures,[17] where they could be used to induce all-optical functional elements. Here it would be very interesting to place a staircase potential obstacle in the path of flowing polaritons. As the polaritons might traverse the obstacle differently depending on whether they arrive from the low-potential or the high-potential side, a tailored asymmetric potential might provide means to create a diode for flowing polaritons.

ACKNOWLEDGMENTS

The Dortmund group acknowledges support through the DFG research Grant No. DFG 1549/15-1. The group at Würzburg University acknowledges support by the State of Bavaria.

[1] A. Demircan, S. Amiranashvili, and G. Steinmeyer, Phys. Rev. Lett. **106**, 163901 (2011).
[2] H. J. Caulfield and S. Dolev, Nature Photon. **4**, 261 (2010).
[3] D. A. B. Miller, Nature Photon. **4**, 3 (2010).
[4] C. Leyder, M. Romanelli, J. P. Karr, E. Giacobino, T. C. H. Liew, M. M. Glazov, A. V. Kavokin, G. Malpuech, and A. Bramati, Nature Phys. **3**, 628 (2007).
[5] C. Adrados, A. Amo, T. C. H. Liew, R. Hivet, R. Houdré, E. Giacobino, A. V. Kavokin, and A. Bramati, Phys. Rev. Lett. **105**, 216403 (2010).
[6] D. Sarkar, S. S. Gavrilov, M. Sich, J. H. Quilter, R. A. Bradley, N. A. Gippius, K. Guda, V. D. Kulakovskii, M. S. Skolnick, and D. N. Krizhanovskii, Phys. Rev. Lett. **105**, 216402 (2010).
[7] A. Amo, T. C. H. Liew, C. Adrados, R. Houdre, E. Giacobino, A. V. Kavokin, and A. Bramati, Nature Photon. **4**, 361 (2010).
[8] T. C. H. Liew, A. V. Kavokin, and I. A. Shelykh, Phys. Rev. Lett. **101**, 016402 (2008).
[9] R. Johne, I. A. Shelykh, D. D. Solnyshkov, and G. Malpuech, Phys. Rev. B **81**, 125327 (2010).
[10] I. A. Shelykh, R. Johne, D. D. Solnyshkov, and G. Malpuech, Phys. Rev. B **82**, 153303 (2010).
[11] C. Adrados, T. C. H. Liew, A. Amo, M. D. Martin, D. Sanvitto, C. Anton, E. Giacobino, A. Kavokin, A. Bramati, and L. Vina, Phys. Rev. Lett. **107**, 146402 (2011).
[12] M. Sich, D. N. Krizhanovskii, M. S. Skolnick, A. V. Gorbach, R. Hartley, D. V. Skryabin, E. A. Cerda-Mendez, K. Biermann, R. Hey, and P. V. Santos, Nature Photon. **6**, 50 (2012).
[13] J. Kasprzak, M. Richard, S. Kundermann, A. Baas, P. Jeambrun, J. M. Keeling, F. Marchetti, M. Szymańska, R. André, J. Staehli, V. Savona, P. B. Littlewood, B. Deveaud, and L. S. Dang, Nature (London) **443**, 409 (2006).
[14] A. Amo, D. Sanvitto, F. P. Laussy, D. Ballarini, E. D. Valle, M. D. Martin, A. Lemaitre, J. Bloch, D. N. Krizhanovskii, M. S. Skolnick, C. Tejedor, and L. Viña, Nature (London) **457**, 291 (2009).
[15] D. Sanvitto, F. M. Marchetti, M. H. Szymańska, G. Tosi, M. Baudisch, F. P. Laussy, D. N. Krizhanovskii, M. S. Skolnick, L. Marrucci, A. Lemaître, J. Bloch, C. Tejedor, and L. Vina, Nature Phys. **6**, 527 (2010).

[16]T. C. H. Liew, A. V. Kavokin, T. Ostatnický, M. Kaliteevski, I. A. Shelykh, and R. A. Abram, Phys. Rev. B **82**, 033302 (2010).
[17]E. Wertz, L. Ferrier, D. D. Solnyshkov, R. Johne, D. Sanvitto, A. Lemaitre, I. Sagnes, R. Grousson, A. V. Kavokin, P. Senellart, G. Malpuech, and J. Bloch, Nature Phys. **6**, 860 (2010).
[18]O. E. Daif, A. Baas, T. Guillet, J.-P. Brantut, R. I. Kaitouni, J. L. Staehli, F. Morier-Genoud, and B. Deveaud, Appl. Phys. Lett. **88**, 061105 (2006).
[19]C. W. Lai, N. Y. Kim, S. Utsunomiya, G. Roumpos, H. Deng, M. D. Fraser, T. Byrnes, P. Recher, N. Kumada, T. Fujisawa, and Y. Yamamoto, Nature (London) **450**, 529 (2007).
[20]S. Utsunomiya, L. Tian, G. Roumpos, C. W. Lai, N. Kumada, T. Fujisawa, M. Kuwata-Gonokami, A. Löffler, S. Höfling, A. Forchel, and Y. Yamamoto, Nature Phys. **4**, 700 (2008).
[21]R. Balili, V. Hartwell, D. Snoke, L. Pfeiffer, and K. West, Science **316**, 1007 (2007).
[22]E. A. Cerda-Méndez, D. N. Krizhanovskii, M. Wouters, R. Bradley, K. Biermann, K. Guda, R. Hey, P. V. Santos, D. Sarkar, and M. S. Skolnick, Phys. Rev. Lett. **105**, 116402 (2010).
[23]A. Amo, S. Pigeon, C. Adrados, R. Houdré, E. Giacobino, C. Ciuti, and A. Bramati, Phys. Rev. B **82**, 081301 (2010).
[24]D. Sanvitto, S. Pigeon, A. Amo, D. Ballarini, M. De Giorgi, I. Carusotto, R. Hivet, F. Pisanello, V. G. Sala, P. S. Guimaraes, R. Houdre, E. Giacobino, C. Ciuti, A. Bramati, and G. Gigli, Nature Photon. **5**, 610 (2011).
[25]L. Ferrier, E. Wertz, R. Johne, D. D. Solnyshkov, P. Senellart, I. Sagnes, A. Lemaitre, G. Malpuech, and J. Bloch, Phys. Rev. Lett. **106**, 126401 (2011).
[26]M. Wouters, I. Carusotto, and C. Ciuti, Phys. Rev. B **77**, 115340 (2008).
[27]A. Baas, K. G. Lagoudakis, M. Richard, R. André, L. S. Dang, and B. Deveaud-Plédran, Phys. Rev. Lett. **100**, 170401 (2008).
[28]M. Wouters, Phys. Rev. B **77**, 121302 (2008).
[29]J.-S. Tempel, F. Veit, M. Aßmann, L. E. Kreilkamp, A. Rahimi-Iman, A. Löffler, S. Höfling, S. Reitzenstein, L. Worschech, A. Forchel, and M. Bayer, Phys. Rev. B **85**, 075318 (2012).
[30]M. Aßmann, J.-S. Tempel, F. Veit, M. Bayer, A. Rahimi-Iman, A. Löffler, S. Höfling, S. Reitzenstein, L. Worschech, and A. Forchel, Proc. Natl. Acad. Sci. USA **108**, 1804 (2011), [http://www.pnas.org/content/108/5/1804.full.pdf+html].
[31]G. Roumpos, W. H. Nitsche, S. Höfling, A. Forchel, and Y. Yamamoto, Phys. Rev. Lett. **104**, 126403 (2010).
[32]T. C. H. Liew and V. Savona, Phys. Rev. Lett. **106**, 146404 (2011).